Activity-dependent BDNF release and TRPC signaling is impaired in hippocampal neurons of *Mecp2* mutant mice

Wei Li[a], Gaston Calfa[a,1], Jennifer Larimore[b], and Lucas Pozzo-Miller[a,2]

[a]Department of Neurobiology, Civitan International Research Center, The University of Alabama at Birmingham, Birmingham, AL 35294; and [b]Biology Department and Neuroscience Program, Agnes Scott College, Decatur, GA 30030

Edited* by Mu-Ming Poo, University of California, Berkeley, CA, and approved September 4, 2012 (received for review March 28, 2012)

Dysfunction of the neurotrophin brain-derived neurotrophic factor (BDNF) is implicated in Rett syndrome (RTT), but the state of its releasable pool and downstream signaling in mice lacking methyl-CpG-binding protein-2 (*Mecp2*) is unknown. Here, we show that membrane currents and dendritic Ca^{2+} signals evoked by recombinant BDNF or an activator of diacylglycerol (DAG)-sensitive transient receptor potential canonical (TRPC) channels are impaired in CA3 pyramidal neurons of symptomatic *Mecp2* mutant mice. TRPC3 and TRPC6 mRNA and protein levels are lower in *Mecp2* mutant hippocampus, and chromatin immunoprecipitation (ChIP) identified *Trpc3* as a target of MeCP2 transcriptional regulation. BDNF mRNA and protein levels are also lower in *Mecp2* mutant hippocampus and dentate gyrus granule cells, which is reflected in impaired activity-dependent release of endogenous BDNF estimated from TRPC currents and dendritic Ca^{2+} signals in CA3 pyramidal neurons. These results identify the gene encoding TRPC3 channels as a MeCP2 target and suggest a potential therapeutic strategy to boost impaired BDNF signaling in RTT.

Rett syndrome (RTT) is caused by loss-of-function mutations in *MECP2*, encoding methyl-CpG-binding protein 2 (1), which regulates expression of multiple genes, including *Bdnf* (2), a modulator of activity-dependent development, function, and plasticity of CNS synapses (3). BDNF dysfunction likely accounts for sensory and motor abnormalities in RTT, including breathing irregularities (4). However, the underlying molecular mechanisms of BDNF dysfunction are unknown. Recombinant BDNF activates a slow nonselective cationic current (I_{BDNF}) in pontine neurons and hippocampal pyramidal neurons, which is mediated by TRPC3–containing channels downstream of tropomyosin-related kinase B (TrkB)/phospholipase C γ (PLCγ) activation (5, 6). In addition, theta-burst stimulation (TBS) of afferent fibers evokes TRPC-like currents in CA1 and CA3 pyramidal neurons that are sensitive to extracellular BDNF scavenging with TrkB-IgG- and shRNA-mediated TRPC3 knockdown (6, 7). Considering that TRPC3 and TRPC6 form heteromultimers (8) and are members of the PLCγ-coupled TRPC subfamily activated by DAG (9) and that both were identified in a comparative microarray study of *Mecp2* null and *MECP2*-overexpressing mouse hypothalami (2), we investigated BDNF signaling through TRPC3/6 channels in CA3 pyramidal neurons of male symptomatic *Mecp2* mutant mice (*Mecp2*$^{-/y}$; Jaenisch strain) (10).

Results and Discussion

Recombinant mature BDNF was pressure-applied from a glass pipette aimed to the apical dendrites of CA3 pyramidal neurons in the presence of TTX to evoke I_{BDNF} and associated dendritic Ca^{2+} signals, as observed in pontine and hippocampal pyramidal neurons (5, 6, 11). A single 30-s BDNF application evoked significantly smaller I_{BDNF} and dendritic Ca^{2+} signals in *Mecp2* mutant neurons from P40–60 male mice, which are in the symptomatic stage (wild type $n = 12$ cells/4 mice; *Mecp2*$^{-/y}$ $n = 8$ cells/4 mice; $P = 0.018$; Mann–Whitney test; Fig. 1 *A* and *B*; *SI Materials and Methods*). The relationship between I_{BDNF} and dendritic Ca^{2+} signals exhibits a significant linear relationship in neurons from both genotypes (wild type $n = 7$ cells/2 mice, $r = 0.617$, $P = 0.0362$; *Mecp2*$^{-/y}$ $n = 7$ cells/2 mice, $r = 0.648$, $P = 0.028$), whereas the correlation between groups was not statistically different ($P = 0.529$; analysis of covariance), suggesting that both features of BDNF-induced responses are equally affected by *Mecp2* deletion (Fig. 1 *C* and *D*). Consistent with the developmental nature of RTT, BDNF-induced currents and dendritic Ca^{2+} signals in *Mecp2* mutant neurons were not significantly affected in P16–17 mice (wild type n = 3 cells/1 mouse; *Mecp2*$^{-/y}$ n = 3 cells/1 mouse; I_{BDNF}, $P = 0.71$; fura-2 ratio, $P = 0.68$; Mann–Whitney test; Fig. S1*C*), a stage before the appearance of overt neurological symptoms.

Because the TRPC3-containing channels known to be necessary for the expression of I_{BDNF} (5–7) are activated by PLCγ-derived DAG (12), we next compared responses evoked by single 30-s applications of the DAG analog 1,2-Dioctanoyl-*sn*-glycerol (DOG) to apical dendrites of CA3 pyramidal neurons. As previously shown for another DAG analog (1-oleoyl-2-acetyl-*sn*-glycerol, OAG) in pontine and hippocampal CA1 pyramidal neurons (5, 6), DOG also evoked membrane currents (I_{DOG}) and dendritic Ca^{2+} signals in CA3 pyramidal neurons (Fig. 1*E*) with a time course similar to those evoked by recombinant BDNF (Fig. S1 *A* and *B*). Importantly, DOG-evoked currents and dendritic Ca^{2+} signals were significantly smaller in *Mecp2*$^{-/y}$ neurons (wild type $n = 15$ cells/8 mice; *Mecp2*$^{-/y}$ $n = 15$ cells/7 mice; $P = 0.0008$ both I_{BDNF} and fura-2 ratio; Mann–Whitney test; Fig. 1*E*). DOG-evoked currents and dendritic Ca^{2+} signals showed a significant linear relationship in both genotypes (wild type $r = 0.64$, $P = 0.0003$; *Mecp2*$^{-/y}$ $r = 0.28$, $P = 0.038$), but their correlation was not statistically different between genotypes ($P = 0.079$; analysis of covariance), suggesting that both features of DOG-induced responses are equally affected by *Mecp2* deletion (Fig. 1*F*), as is the case for BDNF-mediated signals (Fig. 1*D*).

Consistent with the above physiological observations, using well-characterized antibodies for Western immunoblots, we found that BDNF, TRPC3, and TRPC6 protein levels were significantly lower in the hippocampus (Fig. 2 *A–C*), as well as several other brain regions of *Mecp2*$^{-/y}$ mice (Fig. S2 *A* and *B*). Western blots for BDNF show different bands, which represent

Author contributions: W.L., G.C., and L.P.-M. designed research; W.L., G.C., and J.L. performed research; W.L., J.L., and L.P.-M. analyzed data; and W.L., G.C., J.L., and L.P.-M. wrote the paper.

The authors declare no conflict of interest.

*This Direct Submission article had a prearranged editor.

[1]Present address: Instituto de Farmacología Experimental de Córdoba (IFEC), Consejo Nacional de Investigaciones Científicas y Técnicas (CONICET), Departamento de Farmacología, Facultad de Ciencias Químicas, Universidad Nacional de Córdoba, Córdoba (5000) Argentina.

[2]To whom correspondence should be addressed. E-mail: lucaspm@uab.edu

This article contains supporting information online at www.pnas.org/lookup/suppl/doi:10.1073/pnas.1205271109/-/DCSupplemental.

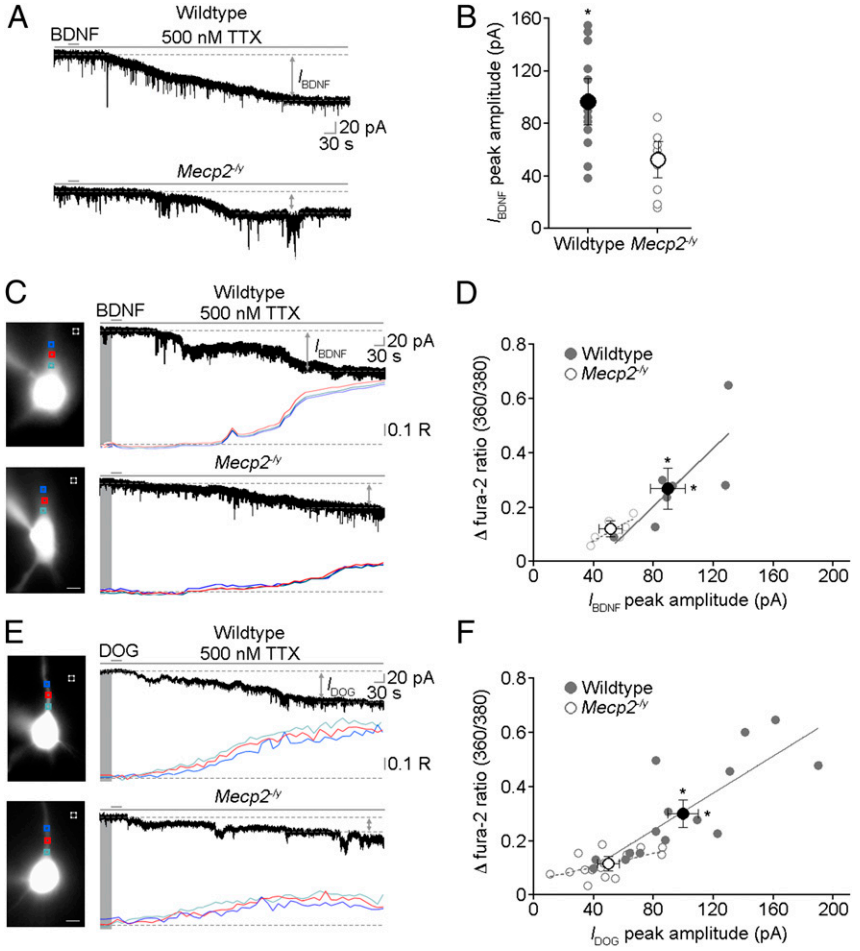

Fig. 1. Membrane currents and Ca^{2+} signals evoked by recombinant BDNF and a TRPC3/6 channel activator are impaired in symptomatic male *Mecp2* mutant mice. (*A*) Representative examples of I_{BDNF} evoked by single 30-s applications of recombinant BDNF to apical dendrites of CA3 pyramidal neurons in the presence of 500 nM TTX (*SI Materials and Methods*). (*B*) Peak I_{BDNF} amplitude is smaller in *Mecp2*$^{-/y}$ neurons. (*C*) Representative examples of I_{BDNF} and simultaneous dendritic Ca^{2+} signals evoked in CA3 pyramidal neurons in the presence of 500 nM TTX (images are neurons loaded with fura-2 and excited at 380 nm; scale bar: 10 μm; R is the 360/380-nm ratio of fura-2 emission). (*D*) Correlation between changes (δ) in fura-2 360/380 ratios and peak I_{BDNF} amplitudes in wild type (gray filled circles) and *Mecp2*$^{-/y}$ neurons (gray open circles). Average changes of fura-2 360/380 ratios and peak I_{BDNF} amplitudes are smaller in *Mecp2*$^{-/y}$ neurons (dark open circle) than in wild-type neurons (dark filled circle). (*E*) Representative examples of currents (I_{DOG}) and Ca^{2+} signals evoked by single 30-s applications of DOG to apical dendrites of CA3 pyramidal neurons in the presence of 500 nM TTX (images are neurons loaded with fura-2 and excited at 380 nm; scale bar: 10 μm). (*F*) Correlation between changes of fura-2 360/380 ratios and peak I_{DOG} amplitudes in wild-type (gray filled circles) and *Mecp2*$^{-/y}$ neurons (gray open circles). Average changes of fura-2 360/380 ratios and peak I_{DOG} amplitudes are smaller in *Mecp2*$^{-/y}$ neurons (dark open circle) than in wild-type neurons (dark filled circle). All data in this and next figures are mean ± SEM; **P* < 0.05 wild type vs. *Mecp2*$^{-/y}$.

monomeric mature BDNF (~14 kDa) and various precursor forms of BDNF, as previously described (13). Mature BDNF bands are the only ones that appear when we performed Western blots with this anti-BDNF antibody on samples of human recombinant mature BDNF at different concentrations, and are completely absent when the anti-BDNF antibody is preabsorbed with recombinant BDNF (Fig. 2*A*). In addition, hippocampal samples from *Mecp2*$^{-/y}$ mice expressed lower levels of *Bdnf* (n = 8, P = 0.045; two-tailed unpaired t test), *Trpc3* (n = 8, P = 0.0074), and *Trpc6* (n = 8, P = 0.0025) mRNAs (Fig. 2 *D*–*F*). These lower *Bdnf*, *Trpc3*, and *Trpc6* expression levels are consistent with a comparative microarray study of hypothalamic samples from *Mecp2* null and *MECP2*-overexpressing mice (2). Furthermore, the levels of BDNF immunoreactivity in the mossy fiber (MF) tract along CA3 *stratum lucidum*—the region of highest BDNF expression in the brain (14, 15)—were significantly lower in *Mecp2* mutant mice (wild type n = 9 mice; *Mecp2*$^{-/y}$ n = 8 mice; P = 0.0002, Mann–Whitney test; Fig. 2*G*).

In agreement with previous reports (16, 17), our chromatin immunoprecipitation (ChIP) assays showed that MeCP2 binds to *Bdnf* at ~0–300 Kb upstream of the transcription start site in hippocampal samples from wild-type mice, whereas the interaction is minimal in *Mecp2* mutant samples (Fig. S2*D*). Next, chromatin fragments immunoprecipitated by MeCP2 antibodies from cerebral cortical and hippocampal samples were amplified by PCR using specific primer pairs spanning ~4.2 kb of the *Trpc3* gene regulatory region (Fig. 2*H*). We found enriched MeCP2 occupancy at 2.4–3.2 kb upstream of the *Trpc3* transcription start site in wild-type samples but no appreciable binding in samples from *Mecp2* mutant mice. On the other hand, a similar ChIP assay using specific primers pairs spanning ~4.0 kb of the *Trpc6* gene regulatory region failed to detect significant MeCP2 occupancy in wild-type or *Mecp2* mutant samples (Fig. S2*E*), suggesting that the reduced levels of TRPC6 mRNA and protein are due to indirect consequences of *Mecp2* deletion. These results strongly suggest that the lower levels of *Trpc3* mRNA in *Mecp2*

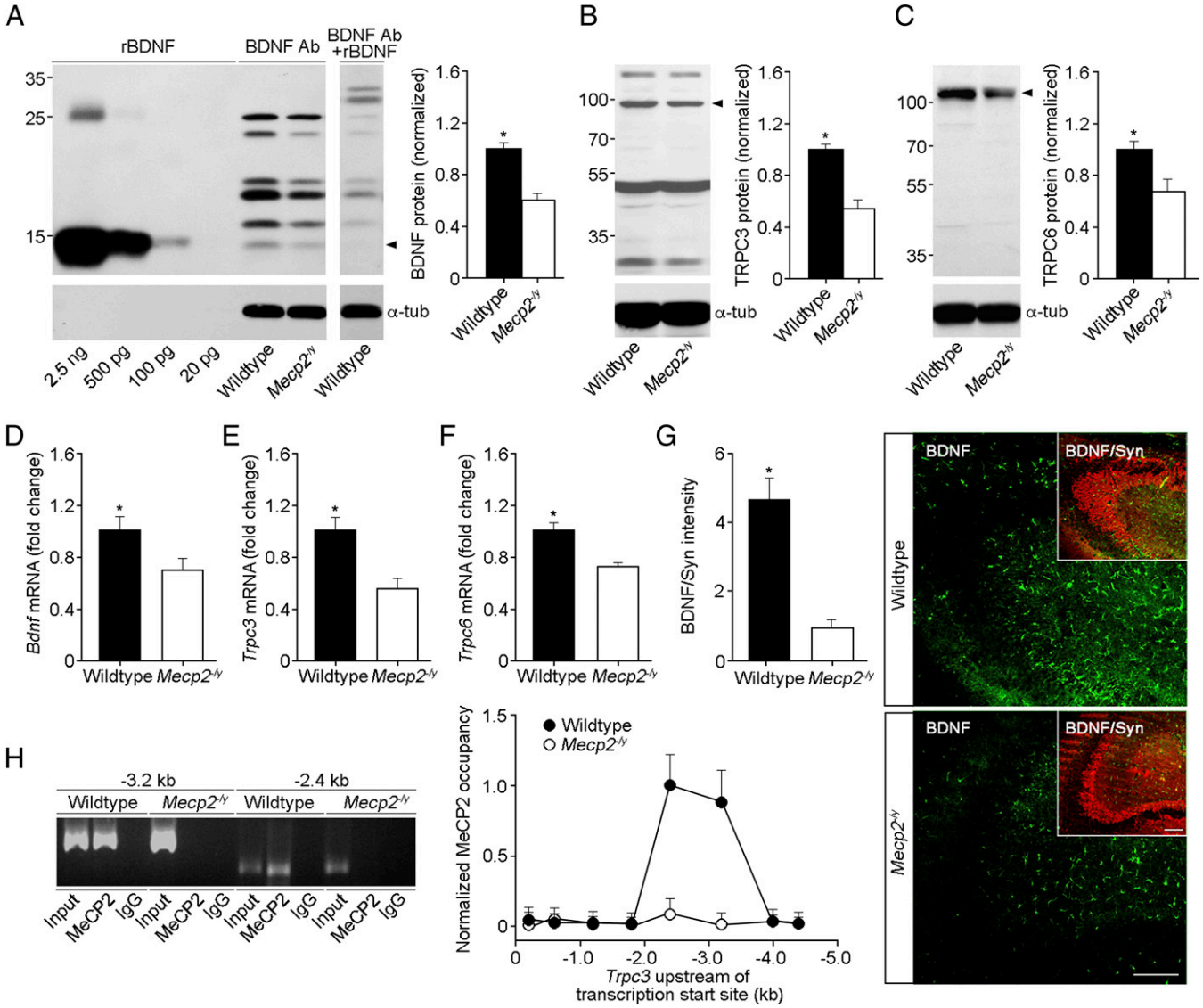

Fig. 2. Expression of BDNF, TRPC3, and TRPC6 is impaired in several brain regions of symptomatic male *Mecp2* mutant mice. (*A–C*) Representative examples of Western immunoblots in hippocampal samples from wild type and *Mecp2*$^{-/y}$ assessed for BDNF (*A*), TRPC3 (*B*), and TRPC6 (*C*) protein levels. (*A*) Western immunoblots were performed in samples of recombinant mature met-BDNF at different concentrations (*Left*), in hippocampal lysates from wild-type and *Mecp2*$^{-/y}$ mice (*Center*), and in hippocampal lysates using primary antibodies preabsorbed with recombinant BDNF (*Right*). Results from quantitative analyses (using α-tubulin as loading control) and shown to the right of the blots demonstrate lower BDNF (*A*), TRPC3 (*B*), and TRPC6 (*C*) levels in the hippocampus of *Mecp2*$^{-/y}$ mice (BDNF, $n = 10$ mice, $P < 0.0001$; TRPC3, $n = 8$ mice, $P < 0.0001$; TRPC6, $n = 7$ mice, $P = 0.018$; two-tailed unpaired *t* test). (*D–F*) Real-time RT-PCR analyses demonstrate lower *Bdnf*, *Trpc3*, and *Trpc6* mRNA levels in the hippocampus of *Mecp2*$^{-/y}$ mice (*Bdnf*, $n = 8$ mice, $P = 0.045$; *Trpc3*, $n = 8$ mice, $P = 0.0074$; *Trpc6*, $n = 8$ mice, $P = 0.0025$; two-tailed unpaired *t* test). (*G*, *Left*) Semiquantitative analysis of BDNF immunoreactivity in the MF tract in CA3 *stratum lucidum*. (*Right*) Representative examples of BDNF and synaptophysin (*Inset*) IHC in area CA3 of hippocampal sections from wild-type (*Upper*) and *Mecp2* mutant (*Lower*) mice. It should be noted that the intensity of synaptophysin immunoreactivity is comparable between genotypes (Scale bar: 10 μm). (*H*, *Left*) Representative examples of agarose gel electrophoresis following ChIP show strong association between MeCP2 and *Trpc3* gene in samples from wild-type mice, which is absent in control IgG and *Mecp2* mutants. (*Right*) Mapping of MeCP2 occupancy at 0.2–4.4 kb upstream of the transcription start site of the *Trpc3* gene. *$P < 0.05$, wild type vs. *Mecp2*$^{-/y}$.

mutant brains are due to direct MeCP2 transcriptional control, identifying *Trpc3* as a gene target of MeCP2 regulation.

What is the physiological consequence of such reduced BDNF, TRPC3, and TRPC6 protein levels in *Mecp2*$^{-/y}$ mice? To address this question, we used membrane currents and dendritic Ca^{2+} signals mediated by TRPC channels as indirect readouts of activity-dependent release of endogenous BDNF (6, 7). A single TBS train to afferent MFs in the presence of a mixture of ionotropic and metabotropic glutamate and GABA receptor antagonists evoked an inward current (MF-I_{BDNF}) in CA3 pyramidal neurons, which outlasted the afferent TBS (Fig. 3*A*; *SI Materials and Methods*), as seen in rat hippocampal slices (7). These TBS-evoked currents have different delay and onset kinetics than the ones evoked by pressure application of recombinant BDNF from a glass pipette onto large areas of the dendritic tree of CA3 pyramidal neurons in slices (Fig. 1 *A* and *B*). The parsimonious explanation for these kinetic differences is that the diffusion of recombinant BDNF from a puffer pipette is very different from the diffusion from BDNF-containing dense-core vesicles within MF terminals. The puffer pipette was positioned several tens of microns above the slice surface to avoid pressure-related mechanical artifacts, and the MF terminals are right across the

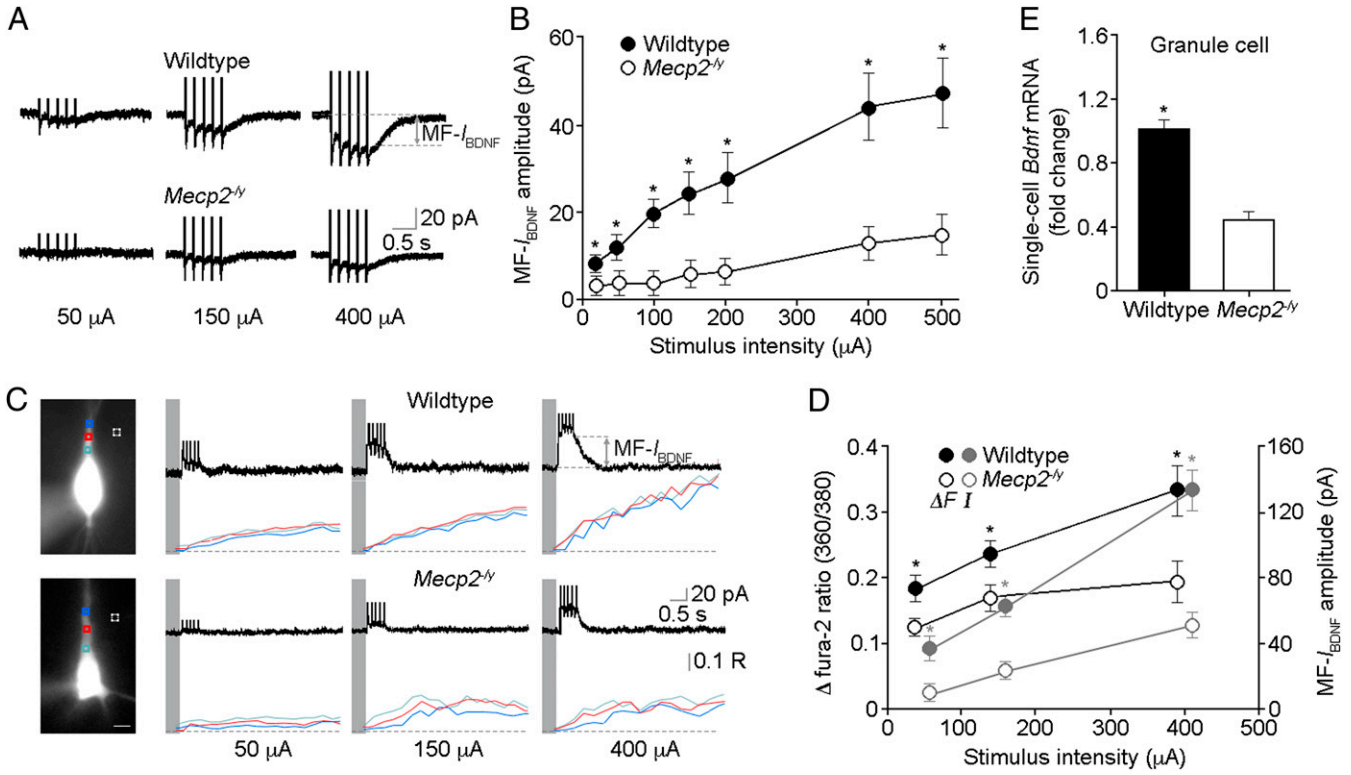

Fig. 3. Membrane currents and Ca^{2+} signals evoked by stimulation of presynaptic MFs are impaired in symptomatic male *Mecp2* mutant mice. (*A*) Representative MF-I_{BDNF} in CA3 pyramidal neurons of wild-type and *Mecp2*$^{-/y}$ mice evoked by TBS of afferent MFs in the presence of a mixture of glutamatergic and GABAergic receptor antagonists (*SI Materials and Methods*). (*B*) Input-output curves of MF-I_{BDNF}. (*C*) Representative images of fura-2-loaded neurons during simultaneous whole-cell recording and Ca^{2+} imaging (380 nm excitation; scale bar: 10 μm; R is the 360/380-nm fura-2 ratio). Fura-2 360/380 ratios were measured from regions of interest (ROIs) over primary dendrites (color-coded in the traces at right); dashed squares are ROIs of background measurements. (*D*) Peak MF-I_{BDNF} amplitude and changes in fura-2 360/380 ratio plotted vs. afferent stimulus intensity. (*E*) Lower levels of *Bdnf* mRNA in individual *Mecp2*$^{-/y}$ granule cells of the dentate gyrus (single-cell real-time RT-PCR), which are presynaptic to CA3 pyramidal neurons in recordings of MF-induced I_{BDNF} (MF-I_{BDNF}). *$P < 0.05$, wild type vs. *Mecp2*$^{-/y}$.

postsynaptic CA3 neurons under recording. This puffer pipette arrangement introduces a delay and slows down the onset of the BDNF responses. It should be noted that membrane currents evoked in CA1 and CA3 pyramidal neurons by pressure application of recombinant BDNF have the same pharmacological profile as those evoked by afferent stimulation in the presence of the glutamatergic and GABAergic receptor antagonist mixture (6, 7).

Increasing stimulus intensities evoked MF-I_{BDNF} responses of progressively larger amplitude in both genotypes, but they were significantly smaller and with a faster decay time in *Mecp2* mutant neurons at all stimulus intensities (wild type $n = 25$ cells/8 mice; *Mecp2*$^{-/y}$ $n = 14$ cells/4 mice; $P < 0.05$ for all groups; Mann–Whitney test; Fig. 3*B*; Fig. S3 *B* and *C*). As with recombinant BDNF-induced I_{BDNF} in presymptomatic mice, there were no significant differences in MF-I_{BDNF} and dendritic Ca^{2+} signals in neurons from P16–17 mice (wild type n = 5 cells/2 mice; *Mecp2*$^{-/y}$ n = 5 cells/2 mice; $P = 0.42$ at 50 μA, $P = 0.31$ at 150 μA, $P = 0.22$ at 400 μA for MF-I_{BDNF}; $P = 0.31$ at 50 μA, $P = 0.15$ at 150 μA, $P = 0.54$ at 400 μA for fura-2 360/380-nm ratios; Mann–Whitney test; Fig. S3*D*). As we showed before in CA1 and CA3 pyramidal neurons of rat hippocampal slices (6, 7), sensitivity to the extracellular BDNF scavenger TrkB-IgG (1 μg/mL) confirmed that MF-I_{BDNF} requires activity-dependent BDNF release ($n = 7$ cells/4 mice, $P < 0.05$ for all groups; two-tailed Wilcoxon matched pairs test; Fig. S4*A*); as a control, a nonspecific human control IgG had no effect on MF-I_{BDNF} (Fig. S4*B*).

To reduce the contribution of voltage-gated Ca^{2+} channels during TBS of afferent MFs, we performed the next series of simultaneous whole-cell recordings and Ca^{2+} imaging at depolarized potentials (+40 mV) with the addition of the L-type Ca^{2+} channel blocker nimodipine in the antagonists mixture (18). Consistently, TBS of MFs evoked outward MF-I_{BDNF} responses (see I-V relationship in ref. 6) and accompanying dendritic Ca^{2+} signals, both of which were significantly smaller in *Mecp2* mutant neurons at all stimulus intensities (wild type $n = 17$ cells/8 mice; *Mecp2*$^{-/y}$ $n = 10$ cells/5 mice; $P < 0.0001$ at 50 μA, $P = 0.0002$ at 150 μA, $P < 0.0001$ at 400 μA for MF-I_{BDNF}; $P = 0.029$ at 50 μA, $P = 0.032$ at 150 μA, $P = 0.019$ at 400 μA for fura-2 360/380nm ratios; Mann–Whitney test; Fig. 3 *C* and *D*). Together, these results demonstrate that MF-I_{BDNF} and associated dendritic Ca^{2+} signals that are sensitive to extracellular BDNF quenching are impaired in *Mecp2* mutant neurons.

Smaller MF-I_{BDNF} could be due to reduced presynaptic BDNF release, impaired postsynaptic TrkB-TRPC signaling, or a combination of both. Compared with the threefold decrease in membrane currents evoked by stimulation of afferent MFs (Fig. 3*B*), I_{BDNF} evoked by recombinant BDNF is only ~twofold smaller in *Mecp2* mutant neurons (Fig. 1*B*), which strongly suggests that activity-dependent release of endogenous BDNF from presynaptic MFs is affected in *Mecp2*$^{-/y}$ mice. Indeed, single-cell real-time RT-PCR demonstrated that *Mecp2* mutant granule cells of the dentate gyrus (which give rise to MFs) expressed lower levels of *Bdnf* mRNA ($n = 12$, $P < 0.0001$; two-tailed unpaired *t* test; Fig. 3*E*; Fig. S2*F*). Consistent with lower levels of BDNF in the extracellular space following TBS of MFs in *Mecp2* mutant slices, a subeffective concentration of the BDNF scavenger TrkB-IgG (0.25 μg/mL) completely blocked MF-I_{BDNF} in *Mecp2* mutant neurons, whereas MF-I_{BDNF} was still detected—albeit reduced—in wild-type neurons (Fig. S5*A*). As a complementary assay for activity-dependent BDNF release, Western blots for phosphorylated

TrkB, PLCγ1, Erk, and Akt in slices that received three TBS trains to MFs in CA3 *stratum lucidum* (30 s intervals) showed no significant increases in either wild-type or *Mecp2*$^{-/y}$ mice (Fig. S5 *B–E*). To avoid the inevitable dilution factor in homogenized hippocampal slices prepared for Western blots, we then performed semiquantitative immunohistochemistry (IHC) with antibodies against phospho-TrkB receptors in slices stimulated as above right before fixation (or were fixed without stimulation, as naïve controls). The intensity of phospho-TrkB staining throughout the MF tract in CA3 *stratum lucidum* was significantly higher in stimulated slices than in naïve control slices (wild-type control $n = 11$ sections/5 mice; wild-type TBS $n = 8$ sections/5 mice; $P = 0.005$, Mann–Whitney test; Fig. 4). Consistently, the intensity of phospho-TrkB IHC after stimulation was significantly lower in *Mecp2* mutant slices than in wild-type slices (*Mecp2*$^{-/y}$ TBS $n = 7$ sections/5 mice; $P = 0.037$; Fig. 4). Furthermore, preincubation with TrkB-IgG (1 μg/mL) prevented the TBS-evoked increase in phospho-TrkB staining (Fig. 4), strongly suggesting that it reflects activity-dependent BDNF release. These observations support the view that activity-dependent BDNF release is impaired in hippocampal slices from *Mecp2* mutant mice.

Altogether, our findings demonstrate impaired BDNF release from presynaptic MFs and postsynaptic TRPC3/6 signaling in *Mecp2* mutant mice, revealing a cellular phenotype that certainly contributes to hippocampal dysfunction in *Mecp2* mutant mice as well as to RTT etiology. BDNF-evoked TRPC3 activation and the resultant Ca^{2+} entry are critical for growth-cone guidance and neuronal survival (19, 20). Dysfunction of this signaling pathway could alter neuronal structure and function and affect the excitation-inhibition balance of neuronal networks as observed in *Mecp2* mutant mice (21) and RTT individuals (22). Lastly, BNDF-induced currents and Ca^{2+} signals are potentially useful as physiological bioassays for the screening and evaluation of therapeutic compounds that enhance BDNF release or boost TRPC3/6 channel function in *Mecp2* mutant mice.

Materials and Methods

Animals. Experimental subjects were hemizygous *Mecp2*$^{tm1.1Jae}$ mutant males of the Jaenisch strain (termed *Mecp2*$^{-/y}$) aged between postnatal days 16 and 17 for the presymptomatic stage and 40 and 60 for the symptomatic stage, when they exhibited RTT-like motor symptoms such as hypoactivity, hind-limb clasping, and reflex impairments (10); age-matched wild-type male littermates were used as the controls. Animals were handled and housed according to the Committee on Laboratory Animal Resources of the National Institutes of Health. All experimental protocols were annually reviewed and approved by the Institutional Animals Care and Use Committee of the University of Alabama at Birmingham.

Acute Hippocampal Slices. Mice were anesthetized with an intraperitoneal (i.p.) injection of a solution of ketamine at 100 mg/mL (wt/vol) per kg of body weight and transcardially perfused with ice-cold "cutting" artificial cerebrospinal

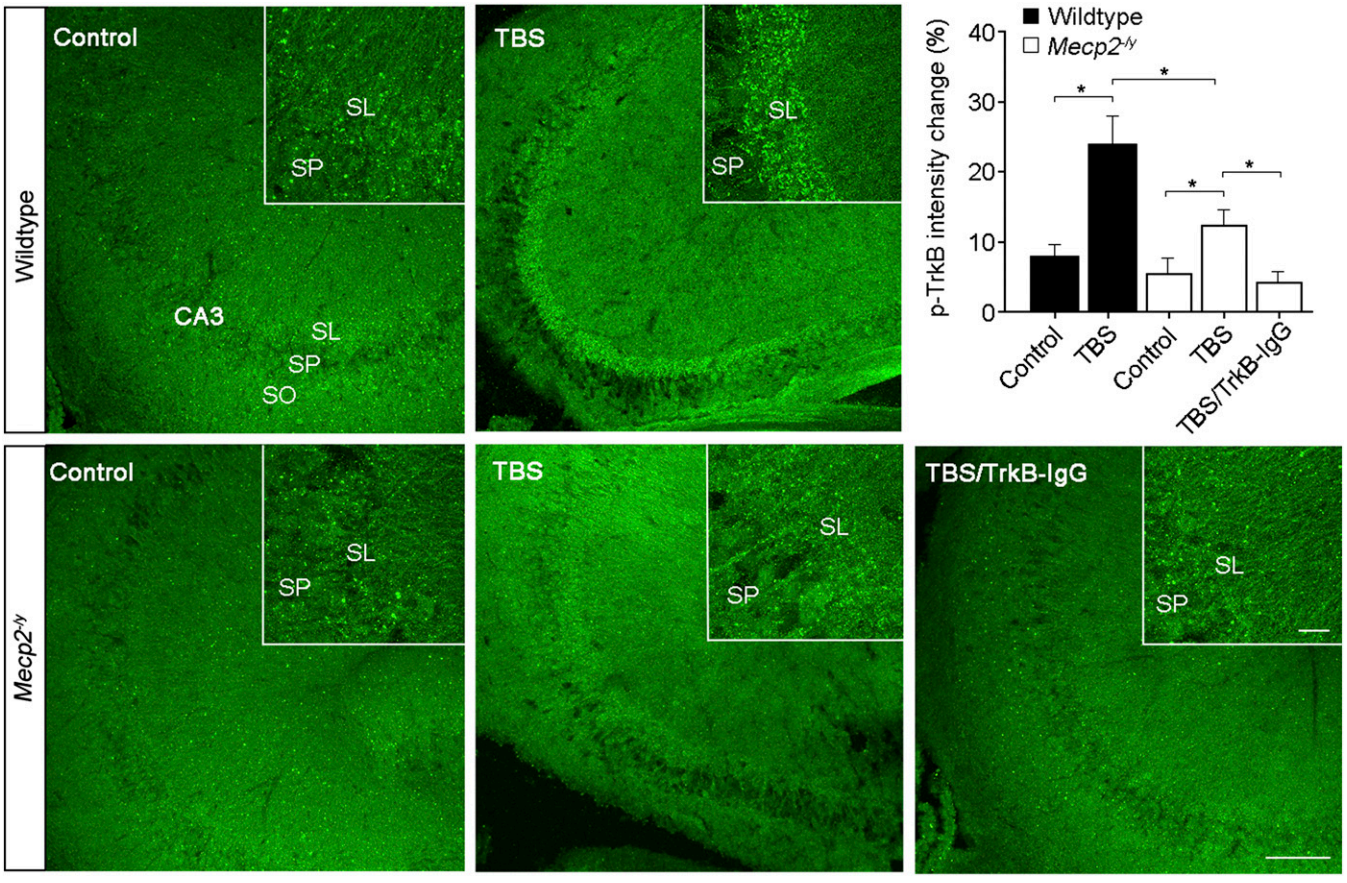

Fig. 4. Activation of TrkB receptors in CA3 *stratum lucidum* following stimulation of MF is impaired in symptomatic male *Mecp2* mutant mice. (*Left*) Representative examples of immunohistochemical labeling with antibodies against phospho-TrkB receptors in acute slices before (control) and after three sets of TBS to the MF tract in CA3 *stratum lucidum* in wild-type (*Upper*) and *Mecp2* mutant mice (*Lower*). (*Right*) Semiquantitative analysis of phospho-TrkB immunoreactivity. The intensity of phospho-TrkB IHC staining after stimulation was significantly lower in *Mecp2* mutant slices than in wild-type slices, although both were increased compared with the naïve controls of the corresponding genotype. Preincubation with the BDNF scavenger TrkB-IgG (1 μg/mL) completely abolished the increase in phospho-TrkB immunoreactivity after TBS in *Mecp2*$^{-/y}$ slices (*Lower Right*). Inset shows higher magnification images from the corresponding sections. SP, *stratum pyramidale*; SL, *stratum lucidum*; SO, *stratum oriens*. (Scale bar: 10μm). *$P < 0.05$.

fluid (aCSF) containing (mM): 87 NaCl, 2.5 KCl, 0.5 $CaCl_2$, 7 $MgCl_2$, 1.25 NaH_2PO_4, 25 $NaHCO_3$, 25 glucose, and 75 sucrose, which was bubbled with 95% O_2/5% CO_2. Hippocampal slices were obtained following standard procedures, as described (21) (*SI Materials and Methods*).

Simultaneous Electrophysiology and Ca^{2+} Imaging. Whole-cell recordings and Ca^{2+} imaging were obtained from visualized CA3 pyramidal neurons after dialysis with intracellular solution containing fura-2, following standard procedures, as described (18) (*SI Materials and Methods*). Recombinant mature BDNF and DOG were pressure-applied from glass pipettes, whereas afferent MFs were stimulated with theta glass pipettes filled with aCSF, as described (6, 7, 11).

Real-Time Reverse Transcription-PCR, Western Immunoblots, Immunohistochemistry, and Confocal Microscopy. Total RNA was extracted from whole hippocampi or from single cells after whole-cell recording, and Reverse Transcription (RT)-PCR was performed following standard procedures. Western immunoblots were also performed following standard procedures. IHC on hippocampal sections from perfused-fixed brains were prepared with a vibrating microtome, acute slices were fixed after afferent stimulation, and semiquantitative confocal microscopy was performed following standard procedures. For details, see *SI Materials and Methods*.

ChIP. ChIP was performed on cerebral cortical and hippocampal samples as described previously with some modifications (*SI Materials and Methods*) (23). PCR was used to amplify different *Bdnf*, *Trpc3*, and *Trpc6* gene regulatory regions, and maximal MeCP2 occupancy was calculated from threshold cycle (Ct) for both wild-type and *Mecp2* mutant mice.

Statistical Analyses. Data for input-output curves of MF-I_{BDNF} and fura-2 ratios and for amplitudes and time courses of membrane currents and fura-2 ratios evoked by recombinant BDNF and DOG were analyzed with one-way repeated measurements ANOVA using Prism software package (GraphPad Software). Specific comparisons between wild-type and *Mecp2*$^{-/y}$ mice were made using Mann–Whitney test. Data for TrkB-IgG and IgG treatments were analyzed with two-tailed Wilcoxon matched pairs test. Data for Western blots, real-time RT-PCR, and IHC were analyzed with two-tailed unpaired *t* test, except otherwise indicated. Linear regressions were made for correlation between fura-2 ratios and peak amplitudes of BDNF- and DOG-evoked currents, and analysis of covariance was used for comparisons between regression lines. Data are shown as the mean ± SEM. Statistical differences were considered significant at $P < 0.05$.

ACKNOWLEDGMENTS. We thank Takafumi Inoue (Waseda University, Tokyo, Japan) for data acquisition and analysis software and Farah Lubin (University of Alabama at Birmingham) for advice and technical assistance with RT-PCR. This work was supported by National Institutes of Health Grants NS-065027 and NS-40593 (to L.P.-M.) and by Postdoctoral Fellowships IRSF-2824 (to W.L.) and IRSF-0804 (to G.C.) from the International Rett Syndrome Foundation. The Alabama Neuroscience Blueprint Core Center (P30-NS57098), the UAB Intellectual and Developmental Disabilities Research Center (P30-HD38985), and the UAB Neuroscience Core (P30-NS47466) provided instrumentation.

1. Amir RE, et al. (1999) Rett syndrome is caused by mutations in X-linked MECP2, encoding methyl-CpG-binding protein 2. *Nat Genet* 23:185–188.
2. Chahrour M, et al. (2008) MeCP2, a key contributor to neurological disease, activates and represses transcription. *Science* 320:1224–1229.
3. Poo MM (2001) Neurotrophins as synaptic modulators. *Nat Rev Neurosci* 2:24–32.
4. Kline DD, Ogier M, Kunze DL, Katz DM (2010) Exogenous brain-derived neurotrophic factor rescues synaptic dysfunction in Mecp2-null mice. *J Neurosci* 30:5303–5310.
5. Li HS, Xu XZ, Montell C (1999) Activation of a TRPC3-dependent cation current through the neurotrophin BDNF. *Neuron* 24:261–273.
6. Amaral MD, Pozzo-Miller L (2007) TRPC3 channels are necessary for brain-derived neurotrophic factor to activate a nonselective cationic current and to induce dendritic spine formation. *J Neurosci* 27:5179–5189.
7. Li Y, Calfa G, Inoue T, Amaral MD, Pozzo-Miller L (2010) Activity-dependent release of endogenous BDNF from mossy fibers evokes a TRPC3 current and Ca2+ elevations in CA3 pyramidal neurons. *J Neurophysiol* 103:2846–2856.
8. Ramsey IS, Delling M, Clapham DE (2006) An introduction to TRP channels. *Annu Rev Physiol* 68:619–647.
9. Hofmann T, et al. (1999) Direct activation of human TRPC6 and TRPC3 channels by diacylglycerol. *Nature* 397:259–263.
10. Chen RZ, Akbarian S, Tudor M, Jaenisch R (2001) Deficiency of methyl-CpG binding protein-2 in CNS neurons results in a Rett-like phenotype in mice. *Nat Genet* 27:327–331.
11. Amaral MD, Pozzo-Miller L (2007) BDNF induces calcium elevations associated with I_{BDNF}, a nonselective cationic current mediated by TRPC channels. *J Neurophysiol* 98: 2476–2482.
12. Putney JW (2005) Physiological mechanisms of TRPC activation. *Pflugers Arch* 451: 29–34.
13. Mowla SJ, et al. (2001) Biosynthesis and post-translational processing of the precursor to brain-derived neurotrophic factor. *J Biol Chem* 276:12660–12666.
14. Danzer SC, McNamara JO (2004) Localization of brain-derived neurotrophic factor to distinct terminals of mossy fiber axons implies regulation of both excitation and feedforward inhibition of CA3 pyramidal cells. *J Neurosci* 24:11346–11355.
15. Dieni S, et al. (2012) BDNF and its pro-peptide are stored in presynaptic dense core vesicles in brain neurons. *J Cell Biol* 196:775–788.
16. Chen WG, et al. (2003) Derepression of BDNF transcription involves calcium-dependent phosphorylation of MeCP2. *Science* 302:885–889.
17. Martinowich K, et al. (2003) DNA methylation-related chromatin remodeling in activity-dependent BDNF gene regulation. *Science* 302:890–893.
18. Pozzo Miller LD, Petrozzino JJ, Golarai G, Connor JA (1996) Ca2+ release from intracellular stores induced by afferent stimulation of CA3 pyramidal neurons in hippocampal slices. *J Neurophysiol* 76(1):554–562.
19. Li Y, et al. (2005) Essential role of TRPC channels in the guidance of nerve growth cones by brain-derived neurotrophic factor. *Nature* 434:894–898.
20. Jia Y, Zhou J, Tai Y, Wang Y (2007) TRPC channels promote cerebellar granule neuron survival. *Nat Neurosci* 10:559–567.
21. Calfa G, Hablitz JJ, Pozzo-Miller L (2011) Network hyperexcitability in hippocampal slices from Mecp2 mutant mice revealed by voltage-sensitive dye imaging. *J Neurophysiol* 105:1768–1784.
22. Glaze DG, et al. (2010) Epilepsy and the natural history of Rett syndrome. *Neurology* 74:909–912.
23. Chao HT, et al. (2010) Dysfunction in GABA signalling mediates autism-like stereotypies and Rett syndrome phenotypes. *Nature* 468:263–269.

Supporting Information

Li et al. 10.1073/pnas.1205271109

SI Materials and Methods

Animals. Breeding pairs of mice lacking exon 3 of *Mecp2* were purchased from the Mutant Mouse Regional Resource Center at the University of California, Davis (B6.Cg-*Mecp2*$^{tm1.1Jae}$, "Jaenisch" strain maintained in C57BL/6 background) (1). A colony was established at the University of Alabama at Birmingham (UAB) by mating wild-type C57BL/6 males with heterozygous *Mecp2*$^{tm1.1Jae}$ mutant females, as recommended by the supplier. Genotyping was performed by PCR of DNA samples from tail clips. Experimental subjects were hemizygous *Mecp2*$^{tm1.1Jae}$ mutant males (termed *Mecp2*$^{-/y}$) aged between postnatal days 16 and 17 for the presymptomatic stage and 40 and 60 for the symptomatic stage, when they exhibited RTT-like motor symptoms such as hypoactivity, hind-limb clasping, and reflex impairments, and wild-type male littermates were used as the controls. Animals were handled and housed according to the Committee on Laboratory Animal Resources of the National Institutes of Health. All experimental protocols were annually reviewed and approved by the Institutional Animals Care and Use Committee of UAB.

Acute Hippocampal Slices. Mice were anesthetized with an i.p. injection of a solution of ketamine at 100 mg/mL (wt/vol) per kg of body weight and transcardially perfused with ice-cold "cutting" aCSF containing (mM): 87 NaCl, 2.5 KCl, 0.5 $CaCl_2$, 7 $MgCl_2$, 1.25 NaH_2PO_4, 25 $NaHCO_3$, 25 glucose, and 75 sucrose, which was bubbled with 95% O_2/5% CO_2. The brain was rapidly removed and cut transversely at 300 μm using a vibrating blade microtome (VT1200S, Leica Microsystems). Slices were transferred to normal aCSF (see below) at 32 °C for 30 min and then allowed to recover at room temperature (24 °C) until use for electrophysiology.

Simultaneous Electrophysiology and Ca^{2+} Imaging. Individual acute slices were transferred to a submerged recording chamber mounted on a fixed-stage upright microscope (Zeiss Axioskop FS) and continuously perfused at room temperature with normal oxygenated aCSF containing (mM): 125 NaCl, 2.5 KCl, 2 $CaCl_2$, 1 $MgCl_2$, 1.25 NaH_2PO_4, 25 $NaHCO_3$, and 25 glucose. Pyramidal neurons in CA3 *stratum pyramidale* were visualized by infrared differential interference contrast microscopy with a water-immersion 63× objective (0.9 NA). I_{BDNF} was recorded in voltage-clamp at a holding potential of -65 mV using unpolished patch pipettes (tip resistance 3–4 MΩ) that contained (mM): 120 Cs-gluconate, 17.5 CsCl, 10 Na-Hepes, 4 Mg-ATP, 0.4 Na-GTP, 10 Na_2-creatine phosphate, and 0.2 Na-EGTA (replaced by 200 μM fura-2 for Ca^{2+} imaging) at 290–300 mOsm and pH 7.4. To reduce the contribution of voltage-gated Ca^{2+} channels during simultaneous whole-cell recording and Ca^{2+} imaging, cells were voltage-clamped at +40 mV. Currents were digitized at 10 kHz and low-pass filtered at 2 kHz. Input resistance (R_i) was measured with hyperpolarizing voltage pulses (50 ms, 20 mV). Cells with series resistances above 15 MΩ were discarded, and cells were also excluded if any whole-cell parameter (i.e., C_m, R_i, R_s) changed by ≥ 20% during the course of an experiment.

Activation of I_{BDNF} by exogenous BDNF was accomplished by pressure application of human recombinant mature BDNF (100 μg/mL, Promega; dissolved in 0.0001% BSA) from a glass pipette (~2 MΩ) connected to a low-pressure regulator and a dry N_2 tank (measured at ~0.4 PSI). Application pipettes were positioned ~50 μm above the slice and ~200 μm away from the soma of the CA3 pyramidal neuron under recording to avoid pressure and mechanical artifacts and were aimed at its apical dendrites within *striatum lucidum* and against the direction of aCSF flow in the recording chamber (2). Each 30-s pulse delivered a maximum of 2 μL of BDNF. Peak I_{BDNF} amplitude was measured after it reached a stable plateau (~15 min) (Fig. S1*A*). The DAG analog 1,2-Dioctanoyl-*sn*-glycerol (DOG; EMD Chemicals) was locally applied to neurons as above to selectively activate channels containing the TRPC3 subunit (3). DOG was prepared as a stock solution of 200 mM in DMSO, stored at -80 °C, and added immediately before each experiment to aCSF to a final concentration of 200 μM for loading to pipettes. Each 30-s pulse delivered a maximum of 2 μL of DOG. DMSO was tested at 0.1% as vehicle control (Fig. S1*B*, *Inset*). All other chemicals, if not indicated, were obtained from Sigma-Aldrich, Calbiochem, or Tocris.

To evoke MF-I_{BDNF} in CA3 pyramidal neurons, TBS generated by an isolated stimulator (ISO-Flex, AMPI) were delivered to MFs via a theta glass pipette filled with aCSF and positioned within the hilus. The identity of MF-evoked responses was routinely confirmed using the group II agonist DCG-IV (1 μM) (4). With this electrode arrangement, DCG-IV reduced EPSCs by 38.6% (wild type n = 6 cells/2 mice) (Fig. S3*A*), indicating that these EPSCs have a major component from MFs plus additional contamination by CA3-CA3 associational/commissural fibers. Thus, we cannot rule out that BDNF is released from sources other than MFs during high-frequency stimulation (in the presence of the glutamatergic and GABAergic receptor antagonist mixture). However, the large content of BDNF within MFs (5, 6) supports the simplest interpretation that they are the source for the endogenous BDNF that activates TRPC currents in CA3 pyramidal neurons. Individual TBS trains were composed of five bursts at 5 Hz, with each burst having four pulses at 100 Hz. MF-I_{BDNF} was isolated in aCSF containing the Na^+ channel blocker TTX (10 nM; to reduce polysynaptic events), the NMDAR antagonist D,L-APV (50 μM), the AMPAR antagonist CNQX (20 μM), the group I mGluR antagonist LY-367385 (100 μM), the $GABA_AR$ antagonist picrotoxin (50 μM), and the L-type Ca^{2+} blocker nimodipine (20 μM). MF-I_{BDNF} was measured between 100 ms after the last TBS stimulus and the time point when currents return to the baseline. TrkB-IgG (1 μg/mL; R&D Systems), a chimeric recombinant protein that scavenges extracellular BDNF (7), was bath-applied to slices for 20 min (Fig. S4*A*), and nonspecific human IgG (1 μg/mL) was used as the control (Fig. S4*B*).

Ca^{2+} imaging was performed by including the fluorescent indicator fura-2 in the intracellular solution (200 μM; InVitrogen). After 30 min of whole-cell access, fura-2 was excited with alternating 360 nm and 380 nm light (12 nm bandwidth, ~2 ms switch) with a galvanometric monochromator (Polychrome IV, TILL Photonics) and detected with a quantitative electron-multiplying CCD camera (QuantEM:512SC, Photometrics). We have established that excitation of fura-2 at 360 nm is more efficient than at 340 nm when using water-immersion objectives (8); thus, we use the isosbestic ratio method (9). To increase acquisition rate during activation of MF-I_{BDNF}, 360 nm excitation frames (50 ms exposures) were obtained at the beginning and the end of a series of 380 nm excitation frames acquired every 0.5 s. For slower I_{BDNF} responses, alternating pairs of 360 nm and 380 nm excitation frames were acquired every 15 s. Background-subtracted fluorescence intensities were measured within regions of interest (ROIs) defined over the proximal and distal portions of primary dendrites. The average ratio of 360 and 380 nm fluorescence within each ROI was used as an estimate of intracellular Ca^{2+} concentration, as these two parameters are directly proportional to each other (10). Electrical and

optical data were acquired on a single G5 Macintosh computer (Apple) running customized software (TI-WorkBench, written by Takafumi Inoue; Waseda University, Tokyo, Japan).

Real-Time RT-PCR. For whole hippocampus real-time RT-PCR, total RNA was extracted using RNeasy Plus Mini Kit (Qiagen). RNA concentrations were determined in a NanoDrop Spectrophotometer (Thermo Scientific). mRNAs were reverse-transcribed using the iScript cDNA Synthesis Kit (Bio-Rad) according to the manufacturer's instructions. PCR amplifications were performed using iQ SYBR Green Supermix (Bio-Rad) at 95 °C for 3 min, followed by 50 cycles of 95 °C for 10 s, 62 °C for 30 s, 72 °C for 45 s, and incubation at 70 °C for 10 min. The following primers were used: *Bdnf* IX: 5′-TGGCTGACACTTTTGAGCAC-3′ (forward), 5′-AAGTGTACAAGTCCGCGTCC-3′ (reverse); *Trpc3:* 5′-AAAGAAAACGATGAGGTGAATGAAG-3′ (forward), 5′-CATAACGAAGGCTGGAGATATCCT-3′ (reverse); *Trpc6:* 5′-GGTGCGGAAGATGCTAGAAG-3′ (forward), 5′-AGCTGGATGGTTGAGGATTG-3′ (reverse); and *β-actin:* 5′-CTGACAGGATGCAGAAGG-3′ (forward), 5′-GAGTACTTGCGCTCAGGA-3′ (reverse).

For single-cell real-time RT-PCR, the cytoplasmic content from individual dentate gyrus granule cells was aspirated into the whole-cell patch pipette and expelled into a 0.2 mL PCR tube followed by DNase I (InVitrogen) treatment to digest genomic DNA. After the RT, two-stage nested PCR was performed (Fig. S2*F*). In the first stage, 5 μL cDNA was amplified for 35 thermal cycles using the following outer primer pairs: *Bdnf* IX: 5′-GGTTCGAGAGGTCTGACGAC-3′ (forward), 5′-CAAAGGCACTTGACTGCTGA-3′ (reverse); and *Gapdh:* 5′-AAGGGCTCATGACCACAGTC-3′ (forward), 5′-ACACATTGGGGGTAGGAACA-3′ (reverse).

In the second stage, 1 μL of the cDNA product from the first stage was amplified for 40 thermal cycles using the following inner primer pairs: *Bdnf* IX: as for whole hippocampus PCR; and *Gapdh:* 5′-ACCCAGAAGACTGTGGATGG-3′ (forward), 5′-GGATGCAGGGATGATGTTC-3′ (reverse).

All primer pairs for single-cell PCR were confirmed to be effective with whole hippocampus mRNAs.

Western Immunoblots. Brain tissues including cerebral cortex, hippocampus, striatum, thalamus, hypothalamus, cerebellum, and brainstem were dissected and homogenized in Nonidet P-40 buffer (20 mM Tris at pH 8.0, 137 mM NaCl, 10% glycerol, 1% Nonidet P-40, 2 mM EDTA) containing protease and phosphatase inhibitors. The homogenates were maintained with constant agitation for 2 h at 4 °C and centrifuged at 12,000 × *g* for 20 min. The supernatants were aspirated and protein concentrations determined by Lowry method. Equal amounts of protein sample were denatured in loading buffer (125 mM Tris at pH 6.8, 20% glycerol, 6% SDS, and 5% 2-mercaptoethanol), boiled for 3 min, and subjected to SDS/PAGE. Proteins were transferred to PVDF membrane and blocked with 5% nonfat milk in TBST (20 mM Tris at pH 7.6, 150 mM NaCl, and 0.1% Tween-20) for 1 h. Membranes were incubated with primary antibodies against BDNF (1:500; Santa Cruz), TRPC3 (1:500; Alomone Labs), TRPC6 (1:1,000; Abcam), phospho-TrkB (1:500, phosph-816Y; Abcam), total-TrkB (1:250; Santa Cruz), phospho-PLCγ1 (1:250; Cell Signaling), total-PCLγ1 (1:1000; Cell Signaling), phospho-Erk (1:1000; Cell Signaling), total-Erk (1:2000; Cell Signaling), phospho-Akt (1:1000; Cell Signaling), total-Akt (1:2000; Cell Signaling), and then with corresponding HRP-conjugated secondary antibodies (Santa Cruz). The proteins were detected using the Pierce ECL Substrate (Thermo Fisher Scientific), and signals were captured on autoradiography film and quantified by computer-assisted densitometry. Membranes were reprobed for the loading control with α-tubulin (InVitrogen) and detected using Odyssey infrared imaging system (Li-Cor Bioscience). Ratios of specific bands to the band of α-tubulin were obtained, and values from *Mecp2*$^{-/y}$ mice were normalized by the wild type. Preabsorbing primary antibodies with recombinant BDNF or the antigenic TRPC3 peptide was performed as specificity controls.

ChIP. ChIP was performed on samples from hippocampal and cerebral cortex, with some modifications from previous reports (11). Fresh samples were incubated in 1% formaldehyde for 10 min at 37 °C to crosslink DNA and its associated proteins. The crosslinked samples were washed three times using ice-cold PBS containing protease inhibitors and homogenized in lysis buffer (10 mM Tris at pH 7.5, 10 mM NaCl, 3 mM $MgCl_2$, 0.5% Nonidet P-40). The lysate was centrifuged at 2,300 × *g* for 5 min at 4 °C, and the nuclei pellet was resuspended in 200 μL nuclear lysis buffer (50 mM Tris at pH 8.0, 10 mM EDTA, 1% SDS) followed by sonication for 5 s twice at power level 3 (Sonic Dismembrator Model 100, Fisher Scientific). The homogenate was digested with 300 U micrococcal nuclease (Worthington) for 7 min at room temperature and centrifuged at 15,700 × *g* for 10 min. The supernatant was diluted 10-fold in CHIP dilution buffer (16.7 mM Tris at pH 8.1, 167 mM NaCl, 1.2 mM EDTA, 0.01% SDS), and 10 μL of this diluted supernatant was kept for input. The remaining of the diluted supernatant was precleared with Salmon Sperm DNA/Protein A Agarose-50% Slurry (Millipore) for 1 h at 4 °C and divided into two fractions for incubation with 5 μg nonspecific rabbit IgG and rabbit anti-MeCP2 (Millipore) at 4 °C overnight. Salmon Sperm DNA/Protein A agarose was then added to collect the antibody/MeCP2/DNA complex. The complex was washed sequentially at room temperature for 5 min once with low salt, high salt, and LiCl wash buffers (Millipore) and twice with TE buffer (10 mM Tris at pH 8.0, 1 mM EDTA). MeCP2/DNA complex was eluted from the antibody by washing twice with 250 μL elution buffer (1% SDS, 0.1 M $NaHCO_3$) for 15 min at room temperature. The combined eluates were added with 20 μL 5 M NaCl, and crossliking was reversed by heating the eluates at 65 °C overnight. The eluates were digested with 2 μL 10 mg/mL Proteinase K (Worthington) for 1 h at 55 °C following addition of 10 μL 0.5 M EDTA, 20 μL 1 M Tris at pH 6.5. DNA was recovered using PCR purification kit (Qiagen). PCR amplifications were performed as described above with annealing temperature 56 °C for *Bdnf*, 65 °C for *Trpc3*, and 57.5 °C for *Trpc6*. The following primers were used to amplify different *Bdnf* gene regulatory regions, as described (12): *Bdnf* (∼–0.5 kb): 5′-GCACCGTGCTCAATACTG-3′ (forward), 5′-TAGGTTCTGGAGGGCTAC-3′ (reverse); (∼–0.3 kb): 5′-GTAGCCCTCCAGAACCTA-3′ (forward), 5′-TTCACGCACACAGAAGCC-3′ (reverse); (∼–0.1 kb): 5′-GGCTTCTGTGTGCGTGAATTTGC-3′ (forward), 5′-AAAGTGGGTGGGAGTCCACGAG-3′ (reverse); and (∼0.1 kb): 5′-TGGACTCCCACCCACTTT-3′ (forward), 5′-GTGGCCGATATGTACTCC-3′ (reverse).

The following primers were used to amplify different *Trpc3* gene regulatory regions: *Trpc3* (∼–4.4 kb): 5′-CCAATCAGGTGCTAGCCAGT-3′ (forward), 5′-TTTGCAACTCTGTTGCTTGG-3′ (reverse); (∼–4.0 kb): 5′-ACCTGCCAAGCAACAGAGTT-3′ (forward), 5′-GCACACCCTGGAGAAGAGTC-3′ (reverse); (∼–3.2 kb): 5′-CCAAGCACACGTCGTATCTG-3′ (forward), 5′-TGTTCACACTGAGCGAGGTC-3′ (reverse); (∼–2.4 kb): 5′-CGTGCTTGGAGATGTGAGAA-3′ (forward), 5′-CTAAATGAGGCTGGCTCCAC-3′ (reverse); (∼–1.8 kb): 5′-GTGGAGCCAGCCTCATTTAG-3′ (forward), 5′-GGCACAGTCAGGTGACAAGA-3′ (reverse); (∼–1.2 kb): 5′-GTCACCTGACTGTGCCTGAA-3′ (forward), 5′-AGATGGAGGTCCCCAGTTCT-3′ (reverse); (∼–0.4 kb): 5′-AGAACTGGGGACCTCCATCT-3′ (forward), 5′-TCTACCCTTTGGGATGTTGC-3′ (reverse); and (∼–0.2 kb): 5′-GCAACATCCCAAAGGGTAGA-3′ (forward), 5′-TCTTTTTGGCTGTCCCAGTC-3′ (reverse).

The following primers were used to amplify different *Trpc6* gene regulatory regions: *Trpc6* (~–4.0 kb): 5′-AGGTGTGCTGTCAGGCTTCT-3′ (forward), 5′-CACACATTGCACCTCACACA-3′ (reverse); (~–3.5 kb): 5′-GGATGCTCGGGATAATTTCA-3′ (forward), 5′-GACCCAACATTTTGCTGCTT-3′ (reverse); (~–3.0 kb): 5′-TTTCGGACCATTTGCTTGAT-3′ (forward), 5′-AAGCCAGAAGATCCTGGACA-3′ (reverse); (~–2.5 kb): 5′-CCAGGATCTTCTGGCTTTCA-3′ (forward), 5′-ACCCCAGGAAAGAAATCAGG-3′ (reverse); (~–2.0 kb): 5′-TTTCTTTCCTGGGGTTTCTG-3′ (forward), 5′-GAATCACAGGAGGCAAAAGC-3′ (reverse); (~–1.5 kb): 5′-CTCCTCTTGCAGGGAAAGTG-3′ (forward), 5′-CCACCCTATGCACACAGAGA-3′ (reverse); (~–1.0 kb): 5′-TAGGGTGGGGAATTTGAATG-3′ (forward), 5′-TTCTCCTTCTTCCACGCTTC-3′ (reverse); and (~–0.5 kb): 5′-TGGCATTCAAATGAATCAGG-3′ (forward), 5′-GGAGAGCCGCTGAAGAGTTA-3′ (reverse).

Analysis for the relative MeCP2 occupancy was based on the Δ–Δ Ct method as described (11). Briefly, Ct obtained from real-time PCR was input into the following formula:

$$\Delta\Delta Ct = \left[Ct^{MeCP2} - \left(Ct^{input} - 6.644\right)\right] - \left[Ct^{IgG} - \left(Ct^{input} - 6.644\right)\right],$$

in which 6.644 ($\log_2 100$) was calculated from the input that represents 1% of starting material, and served as an adjustment. Fold changes were calculated using $2^{-\Delta\Delta Ct}$ for both wild-type and *Mecp2* mutant mice. The relative MeCP2 occupancy for each point was obtained by normalizing each fold change value to the highest one.

IHC and Confocal Microscopy. Following deep anesthesia, mice were transcardially perfused with Ringer's solution. Then, animals were perfused with fixative (4% paraformaldehyde with 0.1% glutaraldehyde). Brains were removed and postfixed for 12–18 h. Using a vibrating microtome, brains were sliced into 60 μm sections and stored in antifreeze (0.1 M sodium phosphate monobasic, 0.1 M sodium phosphate dibasic heptahydrate, 30% ethylene glycol, 30% glycerol) at −20 °C. Brain sections (60 μm) that included the hippocampal formation were incubated in 1% sodium borohydride in PBS for 20 min at room temperature, followed by extensive washing with PBS. Samples were pre-incubated in PBS with 5% NHS and 1% BSA and 0.3% Triton X-100 for 60 min at RT. Samples were incubated overnight in primary antibody solutions of PBS with 1% NHS and 1% BSA: anti-BDNF (1:200; Sigma) and anti-synaptophysin (1:10,000; SY38, Millipore). Sections were then incubated for 60 min in secondary antibodies: anti-mouse Alexa-555 (1:500, for anti-synaptophysin; Invitrogen) and anti-rabbit Alexa-488 (1:500, for anti-BDNF; Invitrogen). After incubation in secondary antibodies, sections were incubated in cupric sulfate for 30 min (3.854 W/V ammonium acetate, 1.596 W/V cupric sulfate in distilled water, pH 5). Sections were washed with PBS and mounted on glass slides with Vectashield (Vector Laboratories). Confocal microscopy for BDNF and synaptophysin IHC was performed in an Axiovert 100 M microscope (Carl Zeiss) with a Plan Apochromat 20× 0.5 NA dry objective and coupled to Argon and HeNe Red lasers; emission filters were BP505–530 and LP560. Z-stacks were acquired using ZEN software (Carl Zeiss). For semiquantitative analysis of BDNF immunoreactivity, dentate gyrus and CA3 regions were imaged from nine brain sections (94 z-planes) from nine *Mecp2*$^{-/y}$ mice and eight brain sections (64 z-planes) from eight age-matched wild-type littermates in two separate experiments. Digital images were analyzed using MetaMorph software (Molecular Devices), by creating ROIs to analyze synaptic regions and cell body regions within the hippocampus. Each ROI was analyzed in the synaptophysin channel and the BDNF channel to determine pixel intensity for each channel in each ROI. BDNF intensity level was normalized to synaptophysin. For phospho-TrkB immunostaining, 300 μm hippocampal slices were collected from the recording chamber following different manipulations and fixed overnight in 4% paraformaldehyde. Fixed hippocampal slices were resectioned into 20 μm sections, permeabilized, and incubated with p-TrkB primary antibodies (1:100; Abcam) and then secondary antibodies conjugated to Alexa-488 (1:500; Invitrogen). Confocal microscopy was performed using a Zeiss 510-META microscope, equipped with 10× and 63× oil-immersion objectives and an Argon laser for excitation. Z-stack images from wild-type and *Mecp2*$^{-/y}$ mice were acquired with the same settings of laser power and PMT voltage and gain for subsequent semiquantitative comparison using ImageJ (NIH). Fluorescence intensity changes in CA3 *stratum lucidum* were obtained by normalizing it with CA3 *stratum oriens*.

Statistical Analyses. Data for input-output curves of MF-I_{BDNF} and fura-2 360/380-nm ratios and for amplitudes and time courses of membrane currents evoked by recombinant BDNF and DOG were analyzed with one-way repeated measurements ANOVA using Prism software package (GraphPad Software). Specific comparisons between wild-type and *Mecp2*$^{-/y}$ mice were made using Mann–Whitney test. Data for TrkB-IgG and IgG treatments were analyzed with two-tailed Wilcoxon matched pairs test. Data for Western blots, real-time RT-PCR, and IHC were analyzed with two-tailed unpaired *t* test, except otherwise indicated. Linear regressions were made for correlation between fura-2 360/380-nm ratio and peak amplitude of membrane currents, and analysis of covariance was used for comparisons between regression lines. Data are shown as the mean ± SEM. Statistical differences were considered significant at $P < 0.05$.

1. Chen RZ, Akbarian S, Tudor M, Jaenisch R (2001) Deficiency of methyl-CpG binding protein-2 in CNS neurons results in a Rett-like phenotype in mice. *Nat Genet* 27: 327–331.
2. Amaral MD, Pozzo-Miller L (2007) TRPC3 channels are necessary for brain-derived neurotrophic factor to activate a nonselective cationic current and to induce dendritic spine formation. *J Neurosci* 27:5179–5189.
3. Thebault S, et al. (2005) Receptor-operated Ca^{2+} entry mediated by TRPC3/TRPC6 proteins in rat prostate smooth muscle (PS1) cell line. *J Cell Physiol* 204:320–328.
4. Toth K, Suares G, Lawrence JJ, Philips-Tansey E, McBain CJ (2000) Differential mechanisms of transmission at three types of mossy fiber synapse. *J Neurosci* 20:8279–8289.
5. Danzer SC, McNamara JO (2004) Localization of brain-derived neurotrophic factor to distinct terminals of mossy fiber axons implies regulation of both excitation and feedforward inhibition of CA3 pyramidal cells. *J Neurosci* 24:11346–11355.
6. Dieni S, et al. (2012) BDNF and its pro-peptide are stored in presynaptic dense core vesicles in brain neurons. *J Cell Biol* 196:775–788.
7. Shelton DL, et al. (1995) Human trks: Molecular cloning, tissue distribution, and expression of extracellular domain immunoadhesins. *J Neurosci* 15:477–491.
8. Pozzo Miller LD, Petrozzino JJ, Golarai G, Connor JA (1996) Ca2+ release from intracellular stores induced by afferent stimulation of CA3 pyramidal neurons in hippocampal slices. *J Neurophysiol* 76(1):554–562.
9. Neher E, Augustine GJ (1992) Calcium gradients and buffers in bovine chromaffin cells. *J Physiol* 450:273–301.
10. Grynkiewicz G, Poenie M, Tsien RY (1985) A new generation of Ca^{2+} indicators with greatly improved fluorescence properties. *J Biol Chem* 260:3440–3450.
11. Chao HT, et al. (2010) Dysfunction in GABA signalling mediates autism-like stereotypies and Rett syndrome phenotypes. *Nature* 468:263–269.
12. Martinowich K, et al. (2003) DNA methylation-related chromatin remodeling in activity-dependent BDNF gene regulation. *Science* 302:890–893.

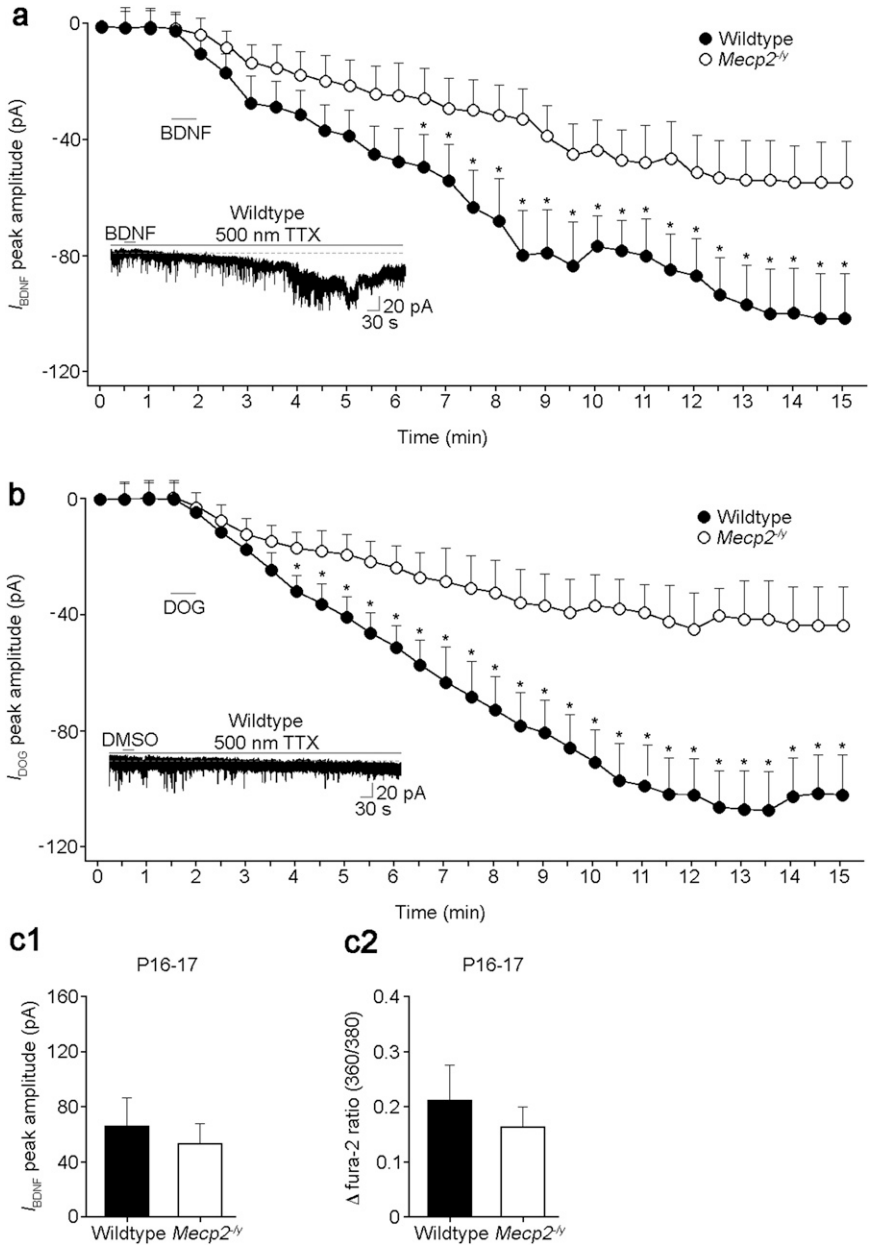

Fig. S1. (*A*) Time courses of I_{BDNF} after a single 30-s pulse of recombinant BDNF application. Compared with wild-type cells, *Mecp2*$^{-/y}$ neurons show smaller I_{BDNF} at about 270 s from BDNF application (wild type, n = 11 cells/4 mice; *Mecp2*$^{-/y}$, n = 11 cells/4 mice; $P < 0.05$ for all groups; Mann–Whitney test). In most cases, BDNF application induced a stable plateau I_{BDNF} level during the 15-min recording, whereas in three cases, I_{BDNF} was recovered by 57.1 ± 6.1% at 600 s after the application. Inset shows a representative example of such a partially reversed I_{BDNF}. (*B*) Time courses of I_{DOG} after a single 30-s pulse of DOG application. Compared with wild-type cells, *Mecp2*$^{-/y}$ neurons show smaller I_{DOG} at about 120 s after DOG application (wild type, n = 15 cells/8 mice; *Mecp2*$^{-/y}$, n = 15 cells/7 mice; $P < 0.05$ for all groups). Inset shows a representative example of whole-cell currents in response to application of 0.1% DMSO as vehicle control; DMSO did not induce any appreciable effects (n = 4 cells/2 mice). In this and all figures, data are shown as the mean ± SEM; *$P < 0.05$, wild type vs. *Mecp2*$^{-/y}$ corresponding time points. (*C*) BDNF-induced currents (*C1*) and dendritic Ca^{2+} (*C2*) signals in CA3 pyramidal neurons from presymptomatic P16–17 mice are comparable to those in wild-type mice.

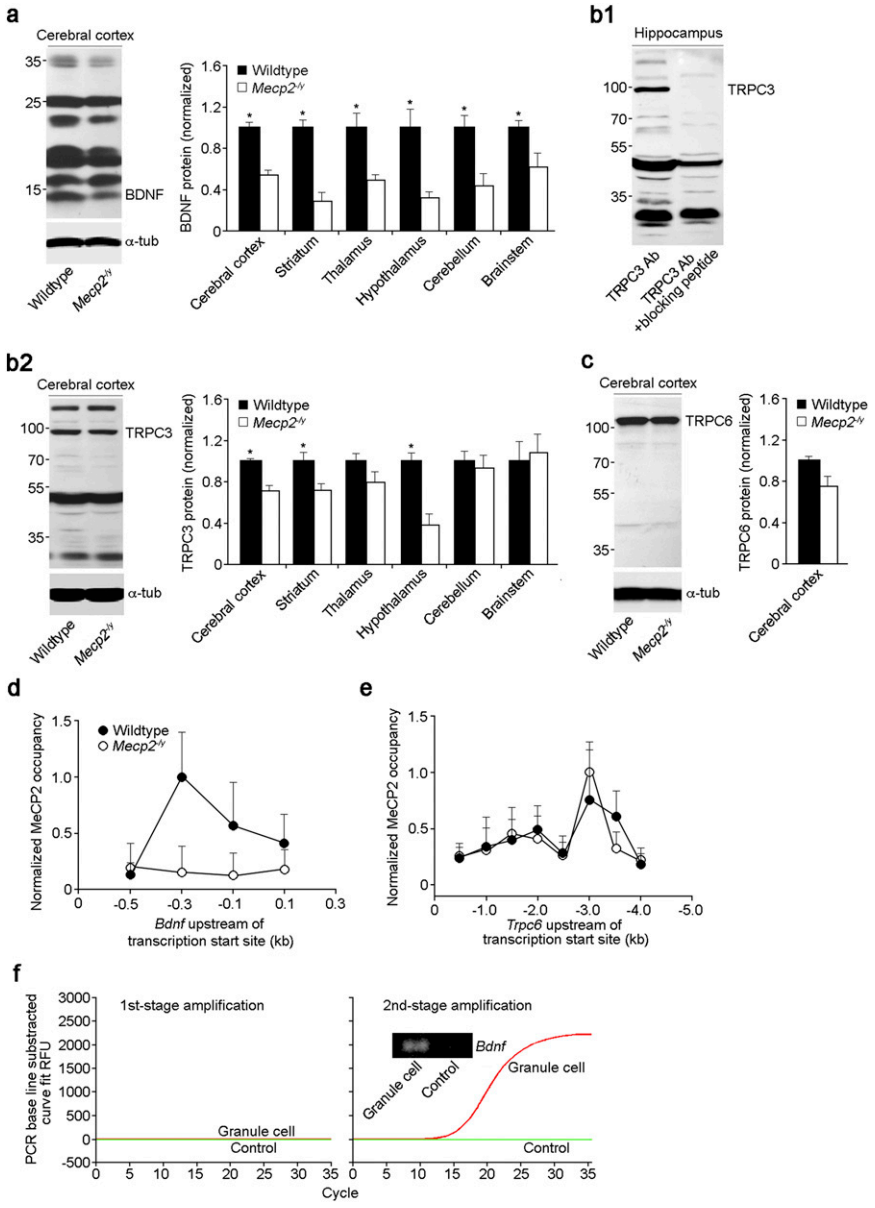

Fig. S2. (*A*, *Left*) Representative examples of Western immunoblots in samples of cerebral cortex from wild-type and *Mecp2*$^{-/y}$ mice assessed for BDNF protein. (*Right*) Quantitative analyses demonstrate lower BDNF protein levels in *Mecp2*$^{-/y}$ mice throughout the brain (cerebral cortex, $n = 10$ mice, $P < 0.0001$; striatum, $n = 5$ mice, $P = 0.005$; thalamus, $n = 10$ mice, $P = 0.0019$; hypothalamus, $n = 5$ mice, $P = 0.043$; cerebellum, $n = 10$ mice, $P = 0.016$; brainstem, $n = 10$ mice, $P = 0.017$; two-tailed unpaired *t* test). (*B1*) Western immunoblots of hippocampal samples show that TRPC3 protein (~100 kDa) was detected by the TRPC3 antibody, whereas it is absent by preincubation with the control peptide antigen (HKLSE KLNPS VLRC, corresponding to residues 822–835 of mouse TRPC3), confirming the specificity of this antibody. (*B2*, *Left*) Representative examples of Western immunoblots in samples of cerebral cortex from wild-type and *Mecp2*$^{-/y}$ mice assessed for TRPC3 protein. (*Right*) Quantitative analyses demonstrate lower TRPC3 protein levels in several brain regions of *Mecp2*$^{-/y}$ mice (cerebral cortex, $n = 8$ mice, $P = 0.0002$; striatum, $n = 5$ mice, $P = 0.035$; hypothalamus, $n = 5$ mice, $P = 0.029$), whereas other regions are unaffected (cerebellum, $n = 8$ mice, $P = 0.68$; thalamus, $n = 8$ mice, $P = 0.17$; brainstem, $n = 8$ mice, $P = 0.78$). (*C*, *Left*) Representative examples of Western immunoblots in samples of cerebral cortex from wild-type and *Mecp2*$^{-/y}$ mice for TRPC6 protein. (*Right*) Quantitative analyses demonstrate lower, albeit not statistically significant ($n = 5$ mice, $P = 0.069$), TRPC6 protein levels in the cerebral cortex of *Mecp2*$^{-/y}$ mice. Data are normalized to α-tubulin (loading control). *$P < 0.05$, wild-type vs. *Mecp2*$^{-/y}$. (*D*) Mapping of MeCP2 occupancy of the *Bdnf* promoter region. MeCP2 significantly interacts with *Bdnf* at ~0–300 kb upstream of the transcription start site in wild-type chromatin samples compared with samples from *Mecp2*$^{-/y}$ mice. (*E*) Mapping of MeCP2 occupancy of the *Trpc6* promoter region. MeCP2 does not interact with *Trpc6* up to ~4.0 kb upstream of the transcription start site in wild-type chromatin samples compared with samples from *Mecp2*$^{-/y}$ mice. (*F*) Single-cell real-time RT-PCR from dentate gyrus granule cells. The cytoplasm of a granule cell in dentate gyrus was collected for singe-cell real-time RT-PCR. BDNF amplification was not evident in the first stage using the outer primer pair (red line, *Left*), whereas it was readily detected in the second stage with the inner primer pair (red line, *Right*). In contrast, no amplification was observed in the control in which all PCR reagents, except for granule cell cytoplasm, were maintained (green lines). The inset shows an agarose gel electrophoresis of the granule cell sample from the second stage confirmed PCR products of the exact BDNF amplicon size, whereas it was absent in the control group. $P < 0.05$, wild type vs. *Mecp2*$^{-/y}$.

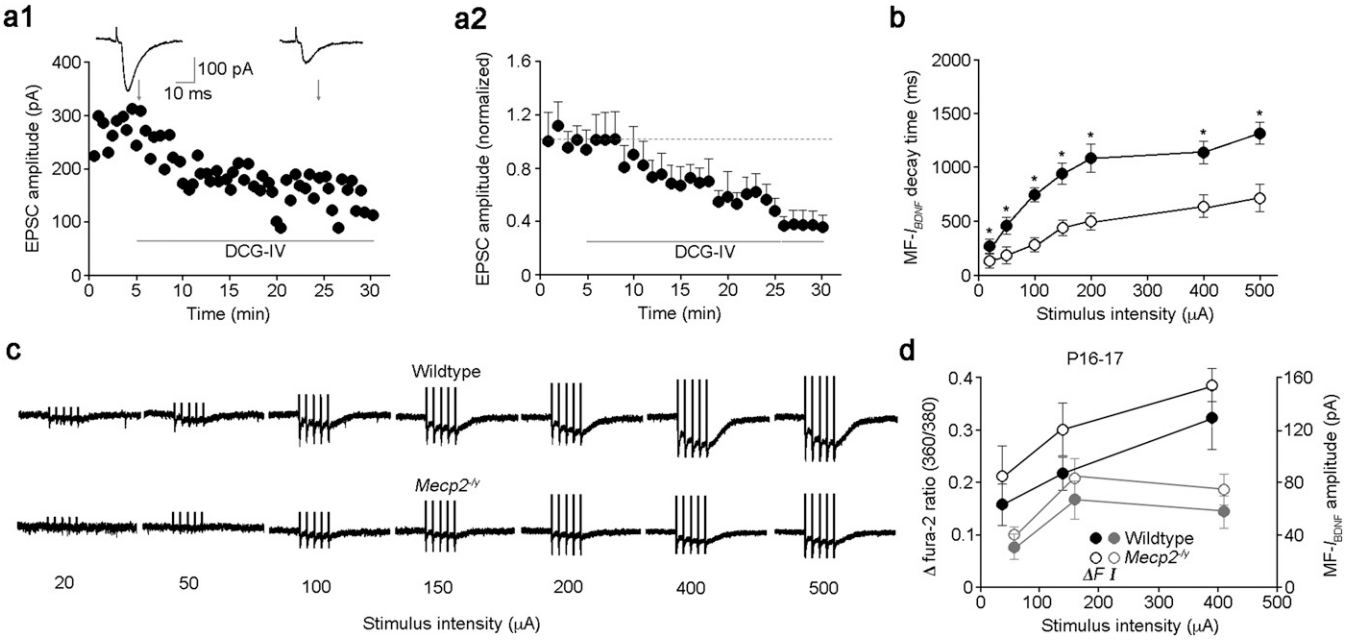

Fig. S3. (*A1*) Representative experiment of the effect of group II mGluR agonist DCG-IV (1 μM; [2S,2′R,3′R]-2-[2′,3′-Dicarboxycyclopropyl]glycine) on EPSC amplitude in CA3 pyramidal neurons. (*Inset*) Representative examples of EPSC before and during DCG-IV application. (*A2*) Group data of the effects of DCG-IV on MF-EPSC amplitude, showing our electrode placement mostly activates MFs. (*B*) Input-output curve of the decay time of MF-I_{BDNF} responses in wild-type and *Mecp2*$^{-/y}$ neurons; decay time was measured between 100 ms after the last stimulus in the TBS and the time point when currents returned to the baseline (wild type, $n = 25$ cells/8 mice, $P < 0.0001$; *Mecp2*$^{-/y}$, $n = 14$ cells/4 mice, $P < 0.0001$; one-way repeated measurements ANOVA). Decay times are significantly shorter in *Mecp2*$^{-/y}$ neurons ($P < 0.05$ for all groups; Mann–Whitney test). *$P < 0.05$, wild type vs. *Mecp2*$^{-/y}$ corresponding stimulus intensity. (*C*) Representative examples of MF-I_{BDNF} evoked with a full range of stimulus intensities from wild-type and *Mecp2*$^{-/y}$ mutant mice in the presence of the glutamatergic and GABAergic receptor antagonists mixture. (*D*) Peak MF-I_{BDNF} amplitude and changes in fura-2 360/380 ratio plotted vs. afferent stimulus intensity in CA3 pyramidal neurons from presymptomatic P16–17 mice.

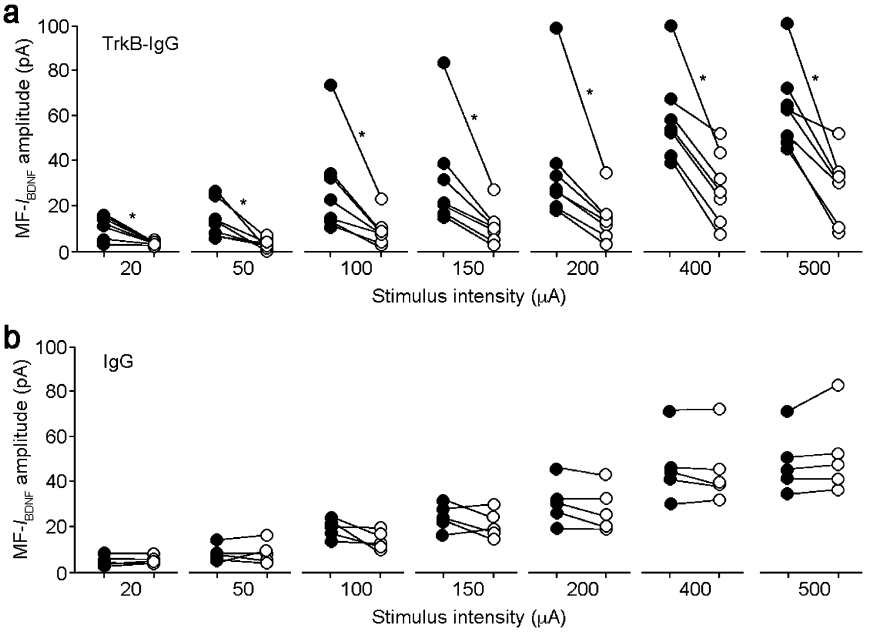

Fig. S4. (*A* and *B*) MF-I_{BDNF} evoked in CA3 pyramidal neurons from wild-type mice using a full range of stimulus intensities were significantly reduced by the extracellular BDNF scavenger TrkB-IgG (*A*; $n = 7$ cells/4 mice, $P = 0.031$ for 20 μA; $P = 0.015$ for other groups; two-tailed Wilcoxon matched pairs test); control nonspecific human IgG had no effect on MF-I_{BDNF} (*B*; $n = 5$ cells/3 mice, $P > 0.05$ for all groups). *$P < 0.05$, pre- vs. posttreatments.

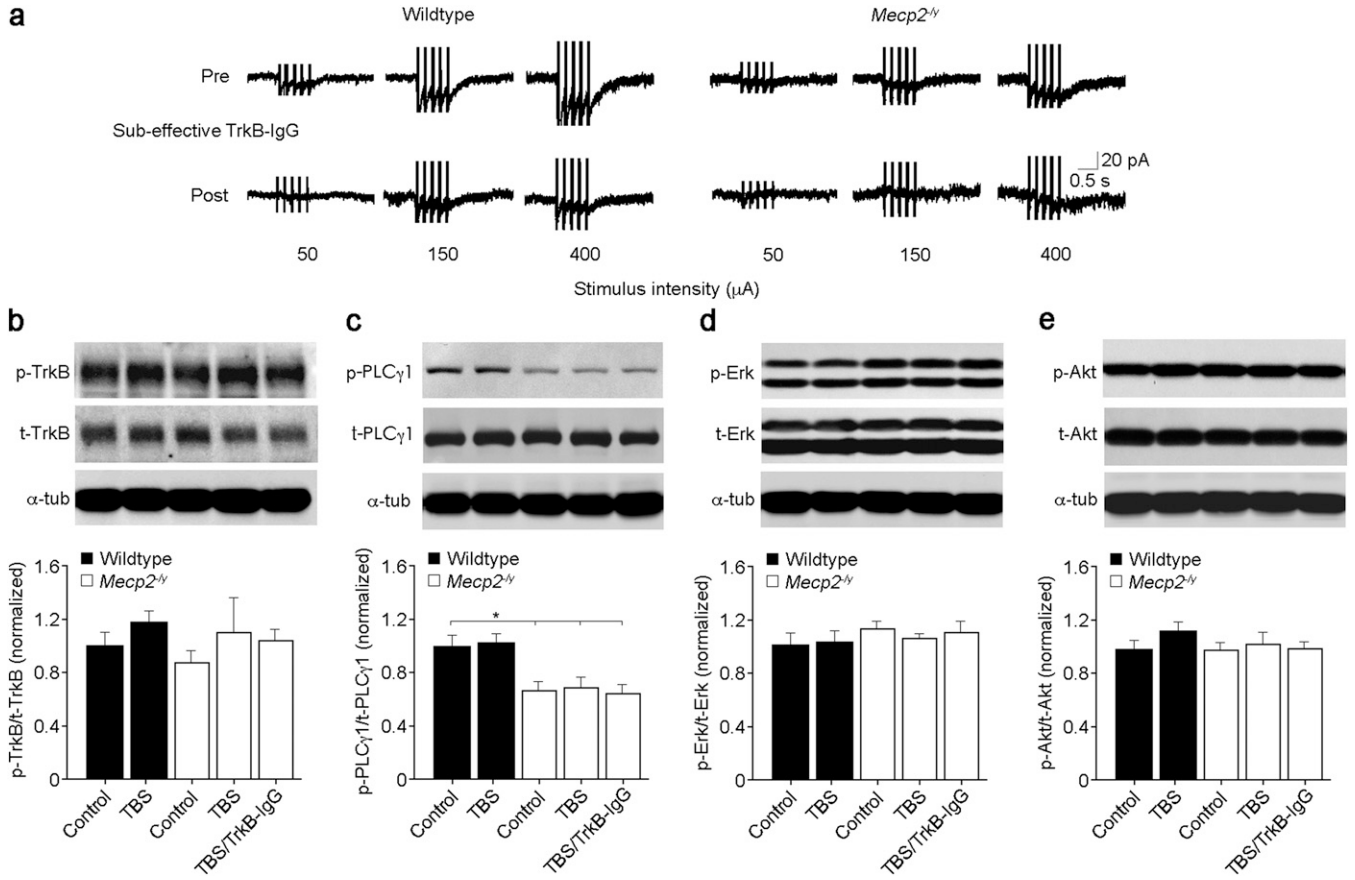

Fig. S5. (*A*) Representative examples of MF-I_{BDNF} evoked with different stimulus intensities from wild-type and *Mecp2* mutant mice in the presence of a subeffective concentration of the BDNF scavenger TrkB-IgG (0.25 μg/mL). Partial BDNF scavenging abolished MF-I_{BDNF} in *Mecp2* mutant slices, but only reduced it in wild-type slices. (*B–E*, *Upper*) Representative examples of Western immunoblots in samples of hippocampal slices that were naïve, stimulated, or stimulated in TrkB-IgG, from either wild-type or *Mecp2* mutant to assay the levels of phospho-TrkB (*B*), phospho-PLCγ1 (*C*), phospho-Erk (*D*), and phospho-Akt (*E*). (*Lower*) Quantitative analyses demonstrate that only phospho-PLCγ1 showed statistically significant differences. *$P < 0.05$, wild-type control vs. *Mecp2*$^{-/y}$ control, TBS, or TrkB-IgG.